A Ferrous-Selective Proximity Sensor for Industrial Internet of Things

M. Adel Ibrahim[1], Galal Hassan[2], Katerina Monea[3], Hossam S. Hassanein[4], Khaled Obaia[5]
[1]*Electrical & computer engineering, Queen's University, Kingston, Canada*
[2,4]*School of computing, Queen's University, Kingston, Canada*
[4]*Oil & Gas, Edmonton, Canada*
[3]*University of Ottawa, Ottawa, Canada*
{[1]mibrahim, [2]ghassan, [4]hossam}@cs.queensu.ca, [3]katmonea@gmail.com, [5]obaia.Khaled@syncrude.com

***Abstract*—This paper presents a ferrous-selective magnetic force proximity sensor (FMPS) for ferrous targets. The proposed simple design utilizes a neodymium magnet and a force sensing resistor. Compared to currently available ferrous-selective inductive proximity sensors (FIPS), FMPS is more power efficient (8 mW) and cost effective. The design can be tweaked to satisfy various application requirements. Experimental results demonstrate the advantages of FMPS-like proximity sensors as it is more suited for energy-constrained wireless sensors (WSs) in Industrial Internet of Things (IIoT) applications.**

***Index Terms*—Industrial Internet of Things (IIoT), proximity, sensor, ferrous, steel, magnet, force sensing resistor, force sensor.**

I. Introduction

With industry 4.0 and 5G networks around the corner, the utilization of wireless technologies is only expected to grow. Industrial Internet of Things (IIoT) applications rely heavily on wireless sensors (WSs) with constrained energy budgets. Such WSs will not be able to host a power-hungry transducer without compromising the sensor's battery lifetime. A number of the well established industrial sensors will have to be redesigned with a particular focus on power efficiency.

One of the commonly used sensors in almost every application domain is the proximity sensor (PS). A PS can be defined as a device used to sense the presence of a physical object (often called a target) in its spacial vicinity. This definition establishes a distinction between PSs and range sensors. While range sensors rely on the same concepts, their targets are not in their spacial vicinity.

Applications of PSs are spread across a wide range of industries. A few examples are: manufacturing, mining, transportation, building automation, and consumer electronics. Their widespread use is rooted in their ability to satisfy common application requirements in motion control, safety [1], access control [2], fault detection [3], interactivity [4], and quality control [5]. As we move towards more automation, the utilization of sensors in general and PSs in particular is only expected to grow.

Proximity sensors sense either active or passive targets. A passive target conveys its presence to the sensor by perturbing a field or interacting with a propagating wave created by the PS. On the contrary, an active target will create such fields and/or waves itself, and the sensor is then used to probe them. Active targets have to be modified or retrofitted with a piece of hardware to make them detectable to their sensors while passive targets does not require any modifications. In industrial applications, passive sensing is preferred because, retrofitting the target with magnets or any other piece of hardware is sometimes not desired or even infeasible. Also, passive sensing reduces the installation overhead incurred by active sensing.

Ferrous-selective PSs are currently available [6] however, their power consumption is too high (typically hundreds of mW) for battery-powered WSs. There is a current need for low-power passive proximity sensors that are selective to ferrous metals (e.g. steel). The only low-power option available commercially is just a detector, not a sensor (i.e., its feedback is binary). Also, it has a relatively small maximum range of 4.29 mm [7].

Ferrous-selective PSs can be useful for monitoring the integrity of steel structures and automating their assembly, monitoring construction equipment, hermetic vessels such as submarines, mining equipment, and aerospace vehicles. They can also be used in process control applications to monitor ferrous-metal machine parts or products on a production line.

We propose a low-power, low-cost, ferrous-selective, passive proximity sensor with a maximum reported range of 20 mm and the option to extend it even more by tweaking the design parameters. The proposed sensor uses a permanent magnet and a Force Sensing Resistor (FSR) to provide a configurable dynamic range with good resolution while consuming significantly less power ($\approx$ 8 mW) [8]. Results indicate very good sensing capabilities with flexible design parameters that can satisfy various requirements.

We begin with the challenges of ferrous-selective PSs for IIoT applications in section II, followed by the classification of proximity sensors in section III. Then we move on to discuss the design of our sensor in section IV, followed by the experimental results in section V. Finally, we conclude the paper in section VI.

II. Challenges in IIoT

Wireless sensing platforms in IIoT applications have their own challenges. In this section we will discuss the major ones related to PSs.

When monitoring construction equipment (e.g., excavators, bulldozers, cranes, etc.) in industrial facilities, it is important to

978-1-7281-5089-5/20/$31.00 ©2020 IEEE

monitor vulnerable steel parts that are exposed to extreme mechanical loads. Ferrous-selective PSs narrows down the sensing capabilities to ferrous metals (i.e., steel). This minimizes false measurements in an environment full of uncertainties and various types of debris.

Wired ferrous-selective PSs introduce a significant challenge by placing delicate electrical wires in an inhospitable harsh environment. Wireless sensing can circumvent this challenge but, has its own challenges, such as the battery lifetime which is a major one. In order for WSs to make economic sense, their battery lifetime has to match or exceed the expected service life of the part being monitored. Also, their cost has to be justified compared to the operational risks they mitigate.

The packaging of a WSs in IIoT applications serves two main purposes. The first is to protect the sensor from all damaging mechanical loads and/or corrosive chemical compounds. With various requirements for the packaging in different applications, it is preferred to have a sensor whose package can be easily reconfigured as needed. The second purpose is to allow for the EM waves to pass with minimal attenuation. This limits the eligible materials to only those with low relative permittivity (ε_r). Composites such as fibreglass, and Kevlar are found to be the best candidates. Although carbon fibre is more mechanically robust, its high relative permittivity [9] disqualifies it.

Wireless signals are reflected by metallic surfaces. With industrial facilities populated with numerous steel structures and equipment, WSs will face a communication challenge. If the WS is deployed inside a metallic enclosure, significant attenuation to its signal is expected. For a wireless standard based on spread spectrum like the low-power long-range wide area network standard (LoRa), the signal can still escape non-hermetic metallic enclosures as shown in [10]. Another way of tackling the communication challenge is by tuning the WS antenna to the metallic structure in its close vicinity. In other words, matching the output impedance of the transceiver to the impedance of the antenna when it is placed inside the non-hermetic metallic enclosure.

The last challenge to be discussed in this section is about security systems. Such systems rely on magnetic field PSs (i.e. reed switches) for access control and tamper detection. A common attack for security systems utilizing a reed switch is the magnetic activation (MA) attack. In this type of attacks, the intruder brings a permanent magnet close enough to the reed switch to keep it in the on-state as its target magnet is moved away. This allows the intruder to gain access without triggering the alarm. Inductive and magnetic force PSs are not prone to this type of attack because, their output is a function of the targets material and precise proximity. This means that they can be calibrated on-site for their own targets. Thus, it becomes extremely hard for an intruder to replicate the exact output of these sensors using a foreign object.

III. Classification of proximity sensors

PSs can be classified according to the physical phenomenon they exploit to sense their targets. Electromagnetic (EM) waves, sound waves, electric fields, and magnetic fields are the four types of physical phenomena governing the operation of PSs as shown in Fig. 1.

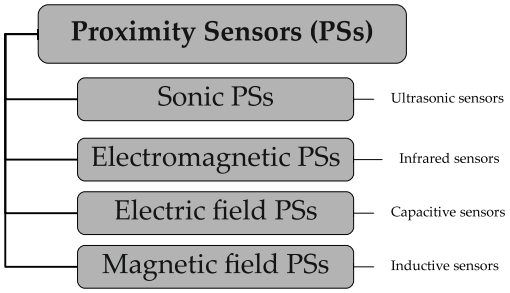

Fig. 1: Classification of proximity sensors based on the physical phenomenon invoked in sensing the proximity of their targets. An example of each class is listed next to it.

Ultrasonic sensors [11] are a clear example of sonic PSs. In this class, sensors are passive and targets are made of sound reflecting materials (almost all solid materials). Underwater sonars work the same way but, they are not considered PSs because, much like electromagnetic radars, their targets are not in their close vicinity.

The class of PSs using EM waves is very common. In this class, proximity sensing depends on one of two methods. In the first method, the sensor measures and analyses an EM wave reflecting off of the target's surface to extract information about its proximity. Photoelectric sensors [12], gesture recognition radar [13], image sensors [14] are all good examples of such method. While aviation radars use the same concept, they are not considered PSs because, their targets are not in their close vicinity. In the second less common method, the sensor radiates an EM wave and measures one of the radiation parameters associated with the proximity of its target. Antenna backscattering is an example of this method. The authors in [15] used a radio frequency identification (RFID) tag to sense the proximity of a target. This was achieved by indirectly measuring the impedance mismatch between the tag antenna and the integrated circuit which is caused by the presence of the target in the close vicinity of the tag antenna.

In the class of electric field PSs, the sensor creates an electric field which gets perturbed by the target causing a shift in the sensor's capacitance. capacitive sensors [16] are the clear example of this class. This class is very popular with different applications in various domains such as object identification in robotics [17].

Finally, magnetic field PSs can sense two types of targets based on their magnetic permeability μ. Targets with high permeability can be either active or passive however, targets with low permeability can only be actively sensed because they have very weak interaction with magnetic fields. Such targets (low μ) are activated by retrofitting them with a permanent magnet and then a Hall-effect sensor or a reed switch on the sensor side can be used to detect the presence of the retrofitted magnet.

Sensing high permeability passive targets is currently done by one of two methods. The first method is called Eddy-current

proximity sensing [18] and, is significantly more popular. It uses a coil to generate a magnetic field which is perturbed when the target is in close vicinity of the coil. This causes a change in the coil's inductance which is then measured by a resonant circuit. This method is utilized by a type of PSs commonly known as inductive sensors [6]. The second method is called DC magnetic sensing which uses a permanent magnet as the source of the field. The magnasphere [7] is an example of this method. It uses a magnetized sphere inside a metal casing as shown in Fig. 2. When the target is within range ($\approx$ 3 mm), the sphere is attracted to the target and moves to the tip of the metal case which in turn creates an electrical connection between the center pin and the case.

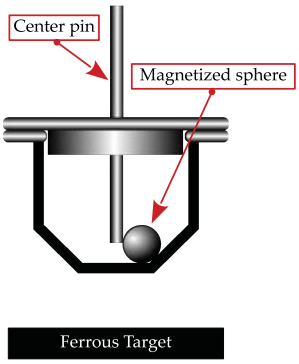

Fig. 2: The MAGNASPHERE ferrous-selective PS [7].

IV. Design

The presented experiment is a design instance of the proposed sensor. The authors believe that other instances with a different layout and/or parameters can be more suitable for other applications.

The design of the proposed magnetic force proximity sensor is shown in Fig. 3. A strong neodymium magnet induces attraction forces between itself and its ferrous target. The FSR is then used to measure the attraction force. The FSR's capacitance is measured instead of its resistance. This is known to improve its accuracy and precision [19]. After calibration for a certain target, a monotonic empirical model can be obtained to express the targets proximity in terms of the FSR's capacitance.

The epoxy layer on top of the FSR has a diameter equal to that of the FSR's active area. This allows the FSR to capture as much as possible of the force exerted by the magnet. While it took numerous trials in the lab to achieve the desired thickness of this layer, it is assumed to be much easier in an automated manufacturing environment.

Since the proximity of the ferrous target is directly related to the attraction force, it is discouraged to have any ferrous object in the vicinity of the PS other than the target itself. This will guarantee that the attraction force between the magnet and the target is the only force being measured by the FSR. Thus, there should be a ferrous free zone around the back of the sensor. The volume of such zone depends on the magnetic field strength of the magnet at its back side. The optimum magnet for this purpose will have a maximum field strength on the side facing its target and no field on the opposite side. Since such idealized permanent magnet doesn't exist, the next best thing is a mounting magnet which is a regular neodymium cylindrical magnet housed inside a special cup that redirects the magnetic flux from the back side to the front side.

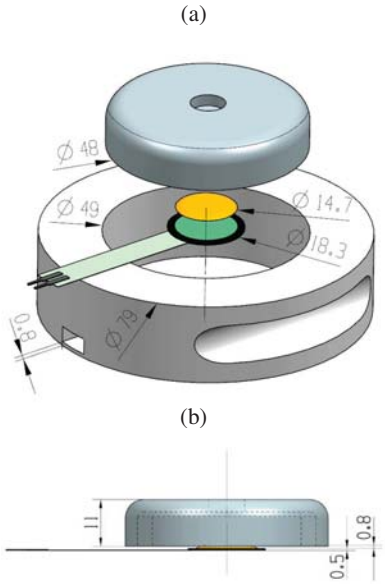

Fig. 3: Sensor design. (a) An isometric exploded view. (b) An orthogonal side view showing the magnet on top, the FSR at the bottom and the epoxy layer between them. Dimensions are in mm.

Magnetostatics simulation tools can simulate and predict the magnetic force if we have good models of the magnet's flux density, the separating medium, and the target's geometry and material composition. Such requirements make simulations only reasonable when a given sensor design has very few use cases in a controlled environment with a fixed target. Even then, considerable discrepancies between simulation results and measurements are expected because of manufacturing tolerances in the magnet and the target, as well as the per component FSR errors [20]. Hence, experimental calibration of the sensor makes more sense for evaluating its performance and characterizing its output in a certain scenario which is the approach followed in this work.

Also, exploiting the magnetic attraction force to sense the proximity of ferrous metals enables the sensor to function effectively even when there are obstacles between the sensor and its target. As long as these obstacles are non-ferrous, it will not affect the sensor's operation. This is not true for inductive sensors because they are also affected by other non-ferrous metals such as aluminium and copper [6].

While some inductive sensors are engineered to be selective for ferrous metals, their cost and power consumption are significantly high compared to the proposed sensor design. Furthermore, a key advantage of the proposed design over mainstream inductive sensors is that it does not produce any electromagnetic interference. The static magnetic field of the

permanent magnet and the FSR are not able to produce propagating electromagnetic waves. This is important when the sensor is embedded in wireless platforms which are expected to be common in IIoT applications. While inductive sensors might require radio frequency (RF) shielding and filtering, the proposed design is inherently non-interfering.

The only foreseeable way this design can produce propagating waves is if the permanent magnet was exposed to high frequency vibrations ($>$ 500 Hz) [21]. Even then, the propagated wave would have a very low frequency which can be easily filtered out by most standard RF filters included in any transceiver.

Some specifications of the given sensor design can be deduced from the specifications of its off-the-shelf components. This allows developers to create a preliminary evaluation of the sensor's performance without having to build a functional prototype. For example, the operating temperature range is simply the intersection of all ranges given by the utilized components (FSR, magnet, etc.). The operating proximity range (P_{op}) can be estimated in two steps. First, with the help of a universal testing machine (UTM) we develop an empirical model of the magnetic attraction force (F) as a function of the target's proximity (P) as shown in Fig. 4. Second, the FSR's minimum and maximum operating forces are superimposed on the curve to identify the proximity range of this setup.

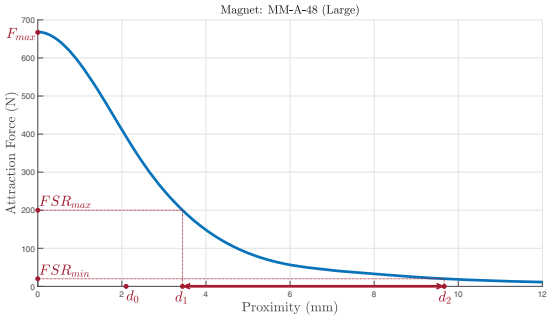

Fig. 4: Empirical model of the magnetic attraction force as a function of the target's proximity.

If $P(f)$ is the target's proximity at $F = f$, then P_{op} can be calculated as follows.

$$P_{op} \in [max(d_0, d_1), d_2] \tag{1}$$

where,

$$d_1 = P(min(FSR_{max}, F_{max}))$$

$$d_2 = P(max(FSR_{min}, W_{mag}))$$

where P_{op} is the operating proximity range. FSR_{max}, FSR_{min} are the maximum and the minimum rated force for the FSR respectively. F_{max} is the maximum attraction force induced by the magnet, which is exerted when the target is in complete contact with the magnet, and W_{mag} is the magnet's weight. d_0 is the distance between the magnet's face and the outer face of the sensor's enclosure. For the design shown in Fig. 3, d_0 is the total sum of the thicknesses of the epoxy layer (0.8 mm), the FSR (0.5 mm), and the bottom surface of the enclosure (0.8 mm) as shown in Fig. 3 (a).

The proposed design can be easily tuned to satisfy different application requirements by changing the magnet and/or the force sensing device. Also, its low-power consumption allows it to be battery powered and embedded in a hermetically sealed wireless module for aerospace, mining, or any other harsh environment application.

V. Experimental Results

In this section we will discuss the experimental work for the proposed sensor and present an evaluation of its performance using different magnets.

A. Setup

A UTM (ZwickRoell Z020) equipped with an accurate load cell ($\pm$0.1 N) was used to benchmark the force measurements collected from the FSR. The speed of the UTM during all the runs was 10 mm/minute with a step resolution of 0.1 mm. The non-ferrous enclosure was 3D-printed with a fused filament fabrication (FFF) 3D-printer using polylactic acid (PLA) filament. The FSR rested on a (0.8 mm) layer of PLA plastic, and its active area was coated with a thin layer (0.8 mm) of epoxy to improve precision [22]. The epoxy layer is the orange coloured layer shown in Fig. 3.

A plastic holder was used to keep the magnet far from the UTM's top clamp (steel) to eliminate any attraction forces between the magnet and the top clamp. A thick ($\approx$ 25 mm) carbon steel target was placed on the bottom. The sensor was positioned such that its bottom surface is parallel to the target's surface.

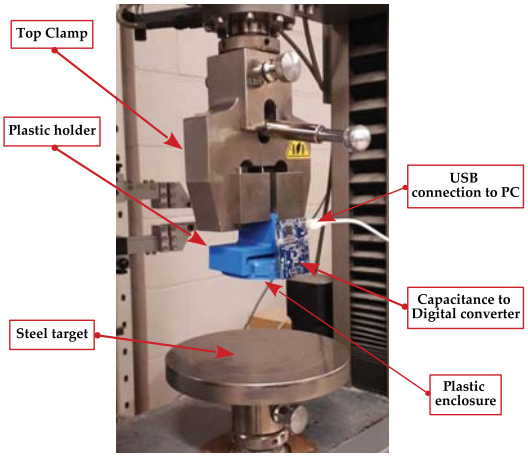

Fig. 5: The experimental setup on the UTM.

In order to quantify the FSR's hysteresis [23], the test was performed in compression mode (approaching) as well as in tension mode (receding). Using a capacitance to digital converter (CDC) [8], the FSR's capacitance was measured instead of its resistance. This was shown to produce more accurate measurements and improve the precision [19].

Three different disc-shaped neodymium magnets of the same grade (N38) were tested to study the effect of the magnet

size on the operating proximity range P_{op}. These magnets were marketed as mounting magnets; their magnetic field has a lot more strength on one side than the other. This helps in reducing the size of the ferrous-free zone at the backside of the sensor. The FSR and the magnets' diameters are listed in Table I.

TABLE I: Components used in the experiment.

Component	Manufacturer	part number	Diameter
Large magnet	K&J Magnetics Inc.	MM-A-48	48 mm
Medium magnet	K&J Magnetics Inc.	MM-A-36	36 mm
Small magnet	K&J Magnetics Inc.	MM-A-20	20 mm
FSR	Interlink Electronics	402	14.7 mm*
CDC	Texas Instruments	FDC2214 [8]	

*diameter of the active area

B. Results and Discussion

The results show good potential for the proposed sensor design. The measurements were post-processed to compensate for the effect of the sensor's weight.

The fundamental laws of magnetism predict the maximum attraction force to be at the smallest separation distance (zero). However, as shown in Figures 6-8, the measured force is not at its maximum when the proximity is zero. We notice the force, as measured by the UTM, start from zero when the target is very far and increases exponentially as it approaches the sensor until it reaches a maximum value at a few millimetres away from the target, then it decreases rapidly till it goes back to zero when the target is in contact with the sensor. This behaviour occurred in both, the approaching and the receding runs.

Careful observation of the experiment's fixtures revealed the reason for this behaviour. As the top clamp of the UTM approaches the bottom target, the attraction force increases and the 3-D printed plastic enclosure experiences significant loading forces. Consequently, the structure flexes and its bottom surface buckles towards the target. As a result, the sensor's enclosure comes into contact with the target before the UTM reaches its calibrated zero position. Once the enclosure is prematurely in contact with the target, the magnetic attraction force starts to be off-loaded to the target, which reduces the amount of force exerted on the UTM's load cell and the FSR. As the proximity gets even closer, more force is off-loaded to the target and even less is applied on the FSR. This behaviour continues until the UTM reaches its calibrated zero position at which there is no buckling in the enclosure. At this point, the load cell of the UTM is measuring zero while the FSR is still squeezed between the magnet and the target. That is why the capacitance does not follow the force all the way down to zero. This effect is severe with the large magnet and diminishes with smaller magnets, as shown in Fig. 9. This is because the distance at which it starts to occur gets smaller as the magnet's size is reduced. A stiffer material for the enclosure than PLA will help minimize this effect when large magnets are used.

As shown in Fig. 6, the capacitance measurements for the large magnet shows an exponential decay similar to that of the force. However, midway through the experiment, it violates the trend with a semi-flat region and then resumes the exponential decay afterwards. A reduced version of this highly non-linear behaviour is noticed in the medium magnet as in Fig. 7 and no such behaviour in the small magnet as in Fig. 8.

Two reasons have contributed to this behaviour. The first reason is that the FSR has been operated beyond its rated maximum force of 20 N. The small magnet is an exception which is why it does not show the same non-linear behaviour. On the other hand, the capacitance of the FSR is monotonically decreasing with proximity. Thus, a single-valued function can be obtained to relate the proximity to the capacitance. This highlights the importance of configuring the sensor design for each application with the appropriate choices of magnets and FSRs to obtain a relatively linear output over its operating range.

The second reason lies with the epoxy resin dome on top of the FSR. While it was reported to improve the FSR's precision [22], in this case, its effectiveness depends on the ratio (R_d) between the magnet's diameter and the diameter of the FSR's active area. Since the resin dome is not perfectly flat, the magnet on top of it can tip slightly, causing it to rest also on the enclosure's bottom surface, not just on the FSR. This behaviour is more likely to occur when the magnet's diameter is a lot bigger than the diameter of the FSR's active area.

In the case of the large magnet in Fig. 6, R_d is 3.28 and the flat region of the curve occupies a large portion of the exponentially decaying part of the curve. As shown in Fig. 7, when R_d got reduced to 2.4 with the medium magnet, the flat region occupied a smaller portion of the curve. Finally, when R_d was further reduced to 1.37 with the small magnet as in Fig. 8, the flat region did not show up at all in the measurements.

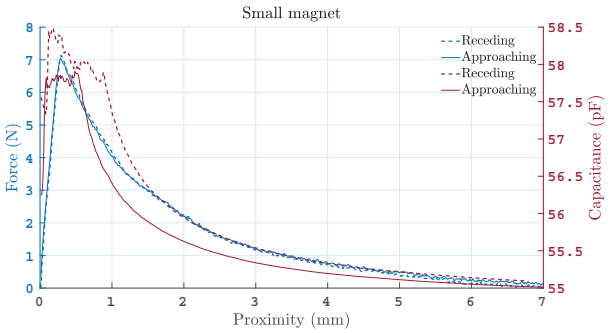

Fig. 6: Target's proximity vs. attraction force (left) and the FSR's capacitance (right) using the large magnet.

In Fig. 9, the small magnet appears to give a relatively small variation in capacitance (≈ 3.5 pF) which can invoke a concern over the resolution of the PS; however, the utilized CDC [8] has a noise floor of 0.3 fF which enables it to quantize the given capacitance range into 11666 levels. This is more than sufficient for providing adequate resolution over the small change in capacitance. Thus the performance limiting factor here remains the accuracy and precision of the FSR, not the CDC. Also, the high sampling rate of the chosen CDC (4.08

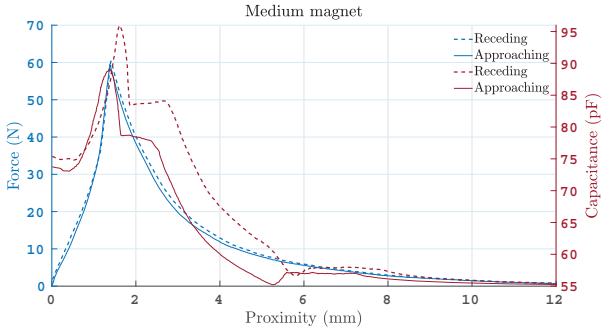

Fig. 7: Target's proximity vs. attraction force (left) and the FSR's capacitance (right) using the medium magnet.

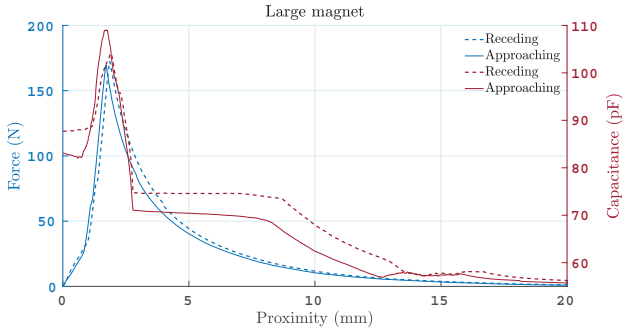

Fig. 8: Target's proximity vs. attraction force (left) and the FSR's capacitance (right) using the small magnet.

ksps) enables the sensor to reliably sense dynamic targets with a response time dictated by the FSR's rise time ($< 3\mu s$). While for static targets, the long term drift of the FSR ($< 5\%$ at 1 kg load for 35 days) is of more concern.

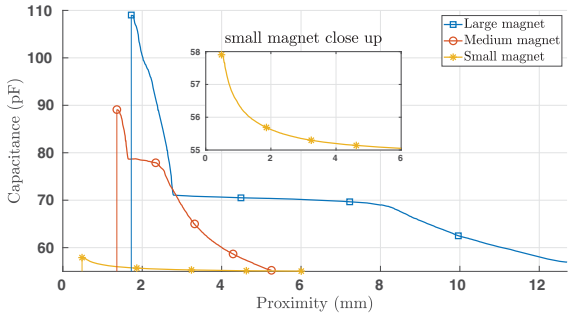

Fig. 9: Output comparison of the three magnets.

VI. Conclusion

In conclusion, The proposed FMPS shows a solid potential for sensing the proximity of ferrous metal targets and it is more suitable for wireless IIoT applications. The FMPS has the advantages of low cost and power consumption (8 mW) compared to the currently existing FIPS. Experimental results showed various operating ranges for different design parameters. The design parameters can be tuned to suit various proximity ranges (10s of millimetres). Experimentation is required to evaluate and characterize its performance for a given target.

References

[1] F. Xia, B. Bahreyni, and F. Campi, "Multi-functional capacitive proximity sensing system for industrial safety applications," in *2016 IEEE SENSORS*, pp. 1–3.

[2] V. K. Sadagopan, U. Rajendran, and A. J. Francis, "Anti theft control system design using embedded system," in *Proceedings of 2011 IEEE International Conference on Vehicular Electronics and Safety*, pp. 1–5.

[3] A. Shahidi, L. A. Gupta, A. Kovacs, and D. Peroulis, "Wireless temperature and vibration sensor for real-time bearing condition monitoring," in *2013 IEEE MTT-S International Microwave Symposium Digest (MTT)*, pp. 1–4.

[4] Y. Wei, R. Torah, Y. Li, and J. Tudor, "Dispenser printed proximity sensor on fabric for creative smart fabric applications," in *2015 Symposium on Design, Test, Integration and Packaging of MEMS/MOEMS (DTIP)*, pp. 1–4.

[5] L. Vojtech, A. M. F. Lopez, M. Neruda, and Z. Lokaj, "Embedded system with RFID technology and inductive proximity sensor," in *2013 36th International Conference on Telecommunications and Signal Processing (TSP)*, pp. 213–217.

[6] S. Fericean and R. Droxler, "New Noncontacting Inductive Analog Proximity and Inductive Linear Displacement Sensors for Industrial Automation," vol. 7, no. 11, pp. 1538–1545.

[7] "MAGNASPHERE: MG-B2-8.0-L." [Online]. Available: https://magnasphere.com/product/l-series/

[8] "Texas instruments: FDC2214." [Online]. Available: http://www.ti.com/lit/ds/symlink/fdc2214.pdf

[9] A. A. Eddib and D. D. L. Chung, "Electric permittivity of carbon fiber," vol. 143, pp. 475–480. [Online]. Available: http://www.sciencedirect.com/science/article/pii/S0008622318310510

[10] M. A. Ibrahim, G. Hassan, H. S. Hassanein, and K. Obaia, "A wireless sensor platform for industrial non-hermetic metallic enclosures," in *2017 13th International Wireless Communications and Mobile Computing Conference (IWCMC)*, pp. 165–170.

[11] C. Canali, G. D. Cicco, B. Morten, M. Prudenziati, and A. Taroni, "A Temperature Compensated Ultrasonic Sensor Operating in Air for Distance and Proximity Measurements," vol. IE-29, no. 4, pp. 336–341.

[12] P. Wei and L. Zhizeng, "A Design of Miniature Strong Anti-jamming Proximity Sensor," in *2012 International Conference on Computer Science and Electronics Engineering*, vol. 3, pp. 327–331.

[13] Project Soli. [Online]. Available: https://atap.google.com/soli/

[14] J. Choi and O. Choi, "Integrated visual sensor with 2D/3D imaging and in-situ proximity sensing for mobile devices," vol. 52, no. 16, pp. 1377–1379.

[15] R. Bhattacharyya, C. Floerkemeier, and S. Sarma, "Low-Cost, Ubiquitous RFID-Tag-Antenna-Based Sensing," vol. 98, no. 9, pp. 1593–1600.

[16] Zhenhai Chen and R. C. Luo, "Design and implementation of capacitive proximity sensor using microelectromechanical systems technology," vol. 45, no. 6, pp. 886–894.

[17] S. Muhlbacher-Karrer, A. Gaschler, and H. Zangl, "Responsive fingers — capacitive sensing during object manipulation," in *2015 IEEE/RSJ International Conference on Intelligent Robots and Systems (IROS)*. IEEE, pp. 4394–4401. [Online]. Available: http://ieeexplore.ieee.org/document/7354001/

[18] P. Ripka, J. Vyhnanek, M. Janosek, and J. Vcelak, "AMR Proximity Sensor With Inherent Demodulation," vol. 14, no. 9, pp. 3119–3123.

[19] A. Matute, L. Paredes-Madrid, E. Gutierrez, and C. A. P. Vargas, "Characterization of drift and hysteresis errors in force sensing resistors considering their piezocapacitive effect," in *2017 IEEE SENSORS*, pp. 1–3.

[20] S. I. Yaniger, "Force Sensing Resistors: A Review Of The Technology," in *Electro International, 1991*, pp. 666–668.

[21] O. C. Fawole and M. Tabib-Azar, "Electromechanically-modulated permanent magnet antennas for wireless communication," in *2017 IEEE SENSORS*, pp. 1–3.

[22] T. R. Jensen, R. G. Radwin, and J. G. Webster, "A conductive polymer sensor for measuring external finger forces," vol. 24, no. 9, pp. 851–858. [Online]. Available: http://www.sciencedirect.com/science/article/pii/0021929091903 10J

[23] L. Paredes-Madrid, A. Matute, and A. Pea, "Framework for a Calibration-Less Operation of Force Sensing Resistors at Different Temperatures," vol. 17, no. 13, pp. 4133–4142.